Optics Letters

Side-lobes-controlled photonic nanojet with a horizontal graded-index microcylinder

Huaming Xing,[1,2] Wenchao Zhou,[1] and Yihui Wu[1,*]

[1]State Key Laboratory of Applied Optics, Changchun Institute of Optics, Fine Mechanics and Physics, Chinese Academy of Sciences, Changchun 130033, China
[2]University of Chinese Academy of Sciences, Beijing 100039, China
*Corresponding author: yihuiwu@ciomp.ac.cn

Received 25 July 2018; revised 8 August 2018; accepted 8 August 2018; posted 9 August 2018 (Doc. ID 340030); published 30 August 2018

A photonic nanojet generated by the transparent dielectric microparticle (microsphere or microcylinder) is a sub-wavelength focused beam. The properties of the photonic nanojet have been modified by changing the refractive index and structure of the micropaticles. In this Letter, a super-narrow photonic nanojet with a full width at half-maximum waist of approximately 116.6 nm ($\lambda/4.3$, with 500 nm excitation wavelength) is obtained by a horizontal graded-index microcylinder, which is divided by multilayers parallel to the direction of light propagation. The method for side lobes controlling by the waves' superposition from the modified graded refractive index and that of the center layer is proposed and discussed. Also, a structure with the composition of different height plates approaching the desired circular section is suggested for decreasing the difficulties in fabrication, and generates a similar photonic nanojet.

OCIS codes: (180.0180) Microscopy; (350.3950) Micro-optics; (260.2110) Electromagnetic optics.

https://doi.org/10.1364/OL.43.004292

A photonic nanojet (PNJ) is a narrow high-intensity focus in the vicinity of the shadow surface of a spherical particle illuminated with a plane wave. Mie theory solving Maxwell's equations with a strict quasi-analytical solution is usually used to explain the scattering of light from the sphere [1]. Applying the method, a PNJ generated by a dielectric sphere was reported by Li *et al.* [2], and Lecler *et al.* analyzed the general three-dimensional properties of the PNJ [3]. The key parameters of the PNJ, which are the position of the focus, the focal spot size, and the maximum intensity of the electric and magnetic fields, have demonstrated mainly dependence on the refractive index and size parameter of the particle [4,5]. The PNJ characterized with excellent optical properties, consisting of low divergence, high intensity, and a sub-diffraction beam width, has been applied in numerous areas, such as Raman signal enhancement, white light nanoscopy, high-density data storage, and direct-write nanopatterning [6–9]. Waist determined by the full width at half-maximum (FWHM) of the PNJ is the most striking and specific feature, which leads to a variety of methods to further reduce the waist [10,11].

Using a pupil mask to cover the center of the microsphere, the FWHM can be reduced around 0.3λ (wavelength λ in free space), but the maximum intensity is weakened [12]. Similarly, the reduced FWHM of 0.374λ and enhanced intensity were generated by pupil-masked 3D dielectric cuboid [13]. A cylindrical metalens assembled by hexagonally arranged nanofibers achieved a reduction of the FWHM of 0.244λ [14]. Also, the PNJs generated by a composite radially inhomogeneous spherical particle and graded-index micro-cuboid have been elongated or confined by different refractive index distributions [15–17]. It is noted that the PNJ generated by the multilayers particle with the refractive index changing radially has been elongated more than confined. To obtain a PNJ with a narrow lateral width, the refractive index of a microparticle is necessarily redistributed.

In this Letter, a side-lobes-controlled ultra-narrow PNJ is generated by a horizontal graded-index microcylinder, which is divided by multilayers parallel to the direction of light propagation. The FWHM of waist 116.6 nm ($\lambda/4.3$, with 500 nm excitation wavelength) is achieved by numerical simulation. The side-lobes-controlled nanojet is obtained with the waves' superposition from a special distribution of the graded index. The effect of the refractive index distribution has been discussed, the graded-index type and the refractive index of the center layer having great influence on the properties of the PNJ. Also, we put forward a structure with the composition of different height plates approaching the cylinder with the desired circular section suggested to decrease the difficulties of fabrication, and get a similar PNJ.

The model for the numerical analysis is shown in Fig. 1. A transparent dielectric microcylinder is considered a 2D structure with several (N) layers of equal thickness d, and the radius of its section is r; the length of the cylinder along the z axis is defined as infinitely long. The mth layer is optically homogeneous and features the refractive index n_m. The structure is illuminated by a monochromatic linearly polarized plane wave propagating along the y axis, and its polarization direction is parallel to the axis of the cylinder, the z axis. The excitation wavelength was taken as 500 nm in free space (refractive index $n_0 = 1$).

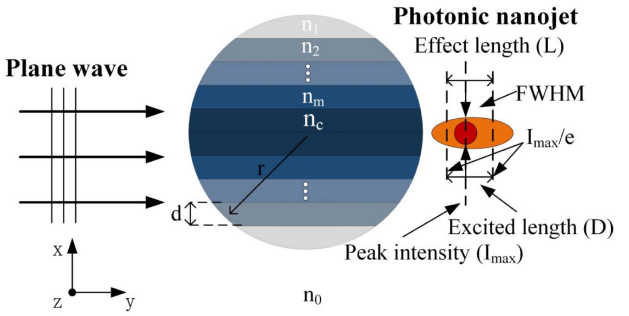

Fig. 1. Schematics of the section of a graded-index microcylinder (layers parallel to the direction of light propagation) used in the simulation.

The refractive index for different layers of a graded-index microcylinder is defined [16], and the refractive index distribution is defined by the equation

$$\frac{n_m}{n_c} = \left(\frac{n_1}{n_c}\right)^{\left(\frac{N-m}{N-1}\right)^g}, \tag{1}$$

where g is the index-grading-type parameter, and m is the mth layer with refractive index n_m; the refractive indices of center layer n_c and outermost layer n_1 values are partly determined by modern coating technology [18]. According to Eq. (1), the refractive index contrast C_m from layer to layer is determined by the formula [16]

$$C_m = \frac{n_m}{n_{m+1}} = \left(\frac{n_c}{n_1}\right)^{\frac{(m+1)^g - m^g}{(N-1)^g}}. \tag{2}$$

The index grading is defined by the g value: linear ($g = 1$), concave ($g < 1$), and convex ($g > 1$).

Analytical methods based on Mie theory and suitable extension are used to calculate the field distribution of homogeneous and concentric or eccentric multilayer microspheres [19–21]. However, the layers along the direction of light propagation make the derivation of an analytical solution intractable. Several methods are used to solve the problem, such as discrete dipole approximation (DDA), finite difference time domain (FDTD), and finite element method (FEM) [22–24]. Here, we calculate the electric field distribution with COMSOL Multiphysics based on FEM, and mesh densities are set to $\lambda/25$ for the model and $\lambda/10$ for the background to guarantee the accuracy of the calculation.

There are two cases regarding the definition of the parameters of the PNJ. When the PNJ is located on the particle surface or inside, the FWHM and the intensity ($|E|^2$) are obtained on the external surface of particles, and the excited length (D) is the distance defined from the particle surface to the point of the intensity equal to the $1/e$ value of peak intensity. The effective length (L) is the distance between the two points where the jet intensity drops by $1/e$ value of peak intensity. Otherwise the FWHM and the $|E|^2$ are calculated at the position of the peak intensity, and the D is equal to the L. The ratio defined by D/L is standing for the percent of the PNJ outside the external surface of the particle.

The radius of the circular section r is 3 μm with six layers of thickness $d = 0.5$ μm. The refractive index of each layer is

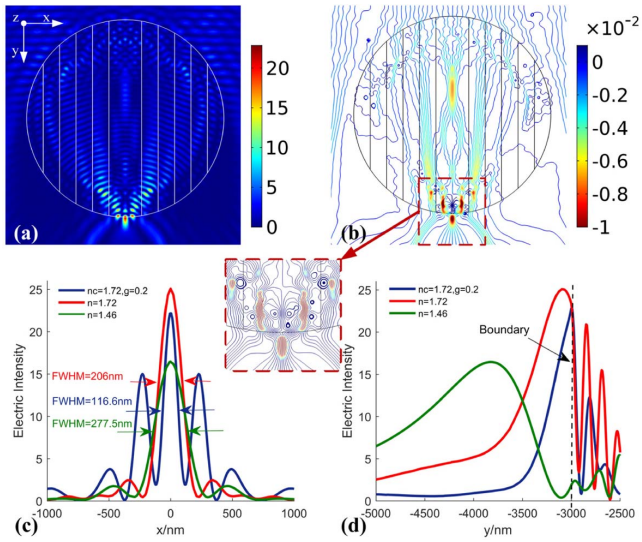

Fig. 2. Electric field intensity distribution for a graded-index microcylinder. (a) Electric field intensity distribution. (b) Streamlines of Poynting vectors. (c) and (d) Transverse and axis intensity profiles of PNJ. The red lines and green lines represent the intensity profile of PNJ generated by a homogeneous microcylinder with refractive indices 1.72 and 1.46, respectively.

defined by Eq. (1), the outermost layer with $n_1 = 1.46$ and center layer with $n_c = 1.72$, and the $g = 0.2$. The electric field intensity distribution is shown in Fig. 2(a). Streamlines of the Poynting vector are depicted in Fig. 2(b), the color scale representing the Py values, and the insert is the zoomed image around the focal region. The FWHM obtained by this geometry is reduced to 116.6 nm ($\lambda/4.3$), compared with the FWHM of 277.5 nm and 206 nm generated by a homogeneous microcylinder with the refractive indices 1.46 and 1.72, respectively, in Fig. 2(c). Similarly, the axis intensity profile of those nanojets is depicted in Fig. 2(d). It is evident that the peak intensity of the nanojet generated by the structure is much closer to the outer surface, compared with the homogeneous microcylinder. Although a part of the PNJ is immersed in the cylinder, the ratio of the PNJ is about 0.822. It means that the majority of the PNJ is excited.

There are two side lobes existing in the vicinity of the central lobe from the electric field intensity in Fig. 2(a). The side lobes corresponding to high spatial frequency are inclined to reduce the length and the width of the PNJ [25]. The narrow PNJ is associated with the presence of side lobes in the vicinity of the central lobe. Also, we can explain the formation of a narrow nanojet from the streamlines of Poynting vectors. There are many vortices in Fig. 2(d), and observed clearly in the zoomed inset image. The Poynting vector in the propagation direction of waves has singular points for a superposition of waves [26]. Those singular points block a part of the intensity of the central lobe, and enhance the intensity of side lobes by the constructive interference of the high-order angular components. In conclusion, it is a superposition of waves that produces singular points around the surface of cylinders to redistribute intensity, leading to side lobes compressing the central lobe. Meanwhile, the singular points inside the particle can induce the curvatures of the PNJ [27].

According to Eq. (1), the refractive index distribution is defined by four parameters, such as the refractive index of the center layer n_c and the outermost layer n_1, the g value, and the number of layers N. The n_1 is determined to be 1.46 by the basic material of glass (silicon dioxide). Under the same conditions with $n_c = 1.72$ and $n_1 = 1.46$, and the g value set to 1, the PNJs are generated by a horizontal graded-index cylinder with a different number of layers. The nanojet generated with layers N from 2 to 6 is slightly confined, and the more layers have little enhancement on the PNJ properties. Thus, the number of layers does not play a major role in the formation of the PNJ generated by the structure, similar to the structure of a core-shell microparticle [15]. Therefore, the following researches focus on a horizontal graded-index microcylinder with six layers.

We first consider the influence of the g value in the formation of a PNJ, under the same condition as Fig. 2(a). The FWHM of the PNJ is reduced with the g value increasing in Fig. 3(a). With the g value increasing, huge side lobes are present to compress the central lobe and weaken the excited intensity. A smaller FWHM of about 105 nm ($\lambda/4.8$) can be obtained with the g equal to 0.3, with a lower intensity than that of the huge side lobes. The smallest FWHM is obtained at $g = 0.4$, but the intensity of the PNJ is almost immersed inside the cylinder. Note that it can be taken as the two nanojets are generated at the situation, similar to the two nanojets obtained by two coherent incident beams [28].

In the same way, we study the effect of n_c, under the same condition as Fig. 2(a). The larger n_c can reduce the width of the PNJ shown in Fig. 3(b). When n_c is equal to 1.6, the nanojet is focused outside of the cylinder, which reduces the side lobes effect in compressing the central lobe. The nanojet with $n_c = 1.64$ is partly immersed inside the cylinder, strongly focused because of the destructive interference of high-frequency components. Here, the whispering gallery mode (WGM) is excited at $n_c = 1.7$. There are three similar nanojets, which means the WGM can enhance the intensity of both the low and high frequency simultaneously. The high-order scattering modes play the dominant role in super-resolution imaging [29]. The WGM generated by the structure probably increases the high-order components to improve the resolution. When n_c is 1.78, several nanojets exist, because of the high refractive index contrast. In conclusion, a PNJ with the smallest width needs to be focused on the external surface of a cylinder, depending on the refractive index of the center layer, and compressed by the side lobes related to the constructive interference of high-frequency components, which is determined by the refractive index of the center layer and the index-grading-type parameter.

In addition, we put forward a structure with the composition of plates to make an approximately desired circular section. The thickness of each plate remains the same as that of layer $d = 0.5$ μm, and the height of each plate is an average with the height of both sides of each layer, except the center layer height is set to 6 μm. The electric field distribution is calculated in Fig. 4(a). Compared with the desired section cylinder, the FWHM of the structure is around 125 nm, slightly bigger than that of the desired section. Furthermore, we increase the height

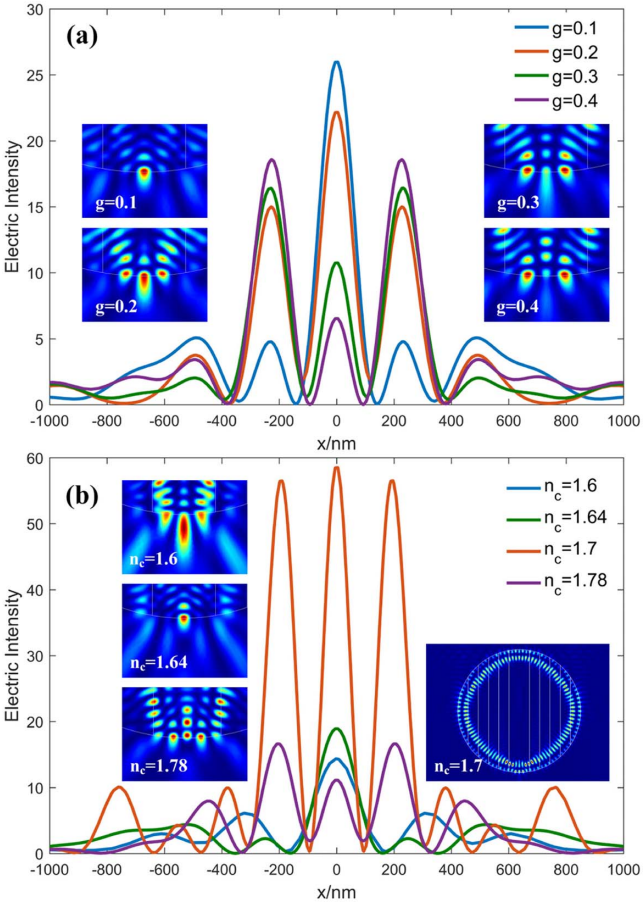

Fig. 3. Refractive index distribution influence on the PNJ properties. (a) and (b) Transverse electric intensity at the focal plane for different g values and for different refractive indices of center layer, respectively. The insets show the details of the intensity distribution.

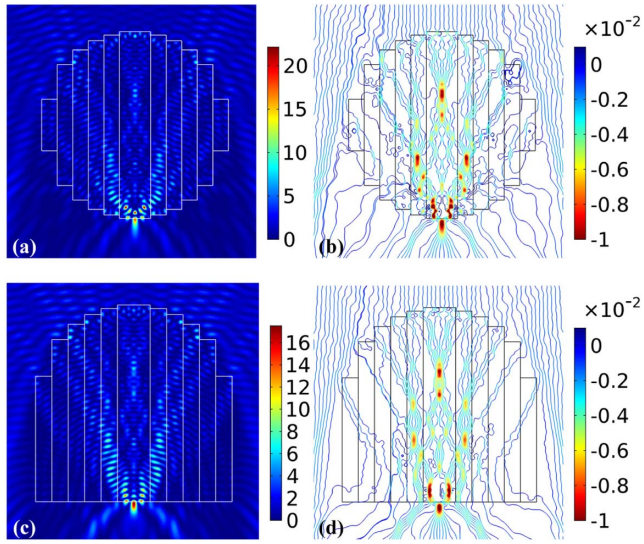

Fig. 4. Structure with the composition of plates. (a) and (c) Electric filed intensity distribution of the structure approaching the whole circle and the structure approaching only the upper half circle with same level in the bottom half of circle. (b) and (d) are the streamlines of the Poynting vector corresponding to structures (a) and (c), respectively. Those simulations are conducted under the same conditions as in Fig. 2(a).

of each layer to reach the same level as the center layer at the bottom. The generated PNJ is shown in Fig. 4(c). The FWHM is around 136 nm, 20 nm larger than that of the desired section. The streamlines of the Poynting vector are shown in Figs. 4(b) and 4(d). The singular points are observed clearly in the vicinity of the central lobe, because of the constructive interference of high-frequency components. In conclusion, the structure with the composition of plates approaching the whole desired circular section or the upper-half section with the same level in the bottom half generates a similar PNJ contrasted to that of the desired section cylinder, suggested to decrease the difficulties of fabrication. Also, varying the composition and porosity of silica glass can make up the controlled synthesis of materials with refractive indices from 1.05 to 2 [30]. The graded index photonic crystal techniques are possible to fabricate the structure as well [31].

In summary, we have presented a horizontal graded-index microcylinder with several homogeneous layers parallel to the direction of light propagation. A PNJ with the FWHM waist of around 116.6 nm ($\lambda/4.3$, with 500 nm excitation wavelength) is obtained with side lobes controlled, which can be explained by the waves' superposition. Through considering the refractive index distribution effect on the PNJ, we can modify the nanojet by controlling the refractive index of the center layer and the g value, getting the smallest FWHM of the PNJ focused on the external surface and compressed by the side lobes. The WGM excited by the structure can enhance the intensity of both the low and high frequencies, which probably increases the high-order components to improve the imaging resolution. Also, we put forward a structure with the composition of different height plates approaching the desired circular section cylinder, suggested to decrease the difficulties of fabrication, and get a similar PNJ. The horizontal grade index design and the mechanism of the waves' superposition can be applied in other structures, such as microspheres, cuboids, and ellipsoids.

Funding. National Natural Science Foundation of China (NSFC) (61504143, 61727813); Technology Development Program of Jilin Province (20160520097JH, 20170414015GH).

REFERENCES

1. G. Mie, Ann. Phys. **25**, 377 (1908).
2. X. Li, Z. Chen, A. Taflove, and V. Backman, Opt. Express **13**, 526 (2005).
3. S. Lecler, Y. Takakura, and P. Meyrueis, Opt. Lett. **30**, 2641 (2005).
4. B. S. Luk'yanchuk, R. Paniagua-Dominguez, I. V. Minin, O. V. Minin, and Z. Wang, Opt. Mater. Express **7**, 1820 (2017).
5. I. V. Minin and O. V. Minin, *Diffractive Optics and Nanophotonics: Resolution Below the Diffraction Limit* (Springer, 2016), 10, 978, p. 31.
6. K. J. Yi, H. Wang, Y. Lu, and Z. Yang, J. Appl. Phys. **101**, 063528 (2007).
7. Z. Wang, W. Guo, L. Li, B. Luk'yanchuk, A. Khan, Z. Liu, Z. Chen, and M. Hong, Nat. Commun. **2**, 218 (2011).
8. S. Kong, A. Sahakian, A. Taflove, and V. Backman, Opt. Express **16**, 13713 (2008).
9. E. Mcleod and C. Arnold, Nat. Nanotechnol. **3**, 413 (2008).
10. H. Zhu, B. Yan, S. Zhou, Z. Wang, and L. Wu, J. Mater. Chem. C **3**, 10907 (2015).
11. Z. Wang, Y. Zhou, and B. Luk'yanchuk, "Near-field focusing of dielectric microspheres: super-resolution and field-invariant parameter scaling," arXiv:1304.4139 (2013).
12. B. Yan, L. Yue, and Z. Wang, Opt. Commun. **370**, 140 (2016).
13. L. Yue, B. Yan, J. N. Monks, Z. Wang, N. T. Tung, V. D. Lam, O. V. Minin, and I. V. Minin, J. Phys. D Appl. Phys. **50**, 175102 (2017).
14. L. Yue, B. Yan, and Z. Wang, Opt. Lett. **41**, 1336 (2016).
15. S. C. Kong, A. Taflove, and V. Backman, Opt. Express **17**, 3722 (2009).
16. Y. Geints, A. Zemlyanov, and E. Panina, J. Opt. Soc. Am. B **28**, 1825 (2011).
17. C. Y. Liu, T. P. Yen, O. V. Minin, and I. V. Minin, Phys. E **98**, 105 (2018).
18. E. Prodan, C. Radloff, N. J. Halas, and P. Nordlander, Science **302**, 419 (2003).
19. G. W. Kattawar, C. Li, P. W. Zhai, and P. Yang, Opt. Express **13**, 4554 (2005).
20. G. Gouesbet and G. Grehan, J. Mod. Opt. **47**, 821 (2000).
21. Y. Shen, L. V. Wang, and J. T. Shen, Opt. Lett. **39**, 4120 (2014).
22. A. Taflove and S. C. Hagness, *Computational Electromagnetics: The Finite-Difference Time-Domain Method* (Artech House, 2005).
23. Y. E. Geints, I. V. Minin, E. K. Panina, A. A. Zemlyanov, and O. V. Minin, Opt. Quantum Electron. **49**, 1 (2017).
24. P. K. Upputuri, M. Krisnan, and M. Pramanik, J. Biomed. Opt. **22**, 045001 (2017).
25. A. Devilez, B. Stout, N. Bonod, and E. Popov, Opt. Express **16**, 14200 (2008).
26. Y. Ben-Aryeh, Appl. Phys. B **84**, 121 (2006).
27. L. Yue, O. V. Minin, Z. Wang, J. N. Monks, A. S. Shalin, and I. V. Minin, Opt. Lett. **43**, 771 (2018).
28. A. Poteet, X. A. Zhang, H. Nagai, and C. H. Chang, Nanotechnology **29**, 075204 (2018).
29. S. Zhou, Y. Deng, W. Zhou, M. Yu, H. P. Urbach, and Y. Wu, Appl. Phys. B **123**, 236 (2017).
30. J. Poco and L. Hrubesh, "Method of producing optical quality glass having a selected refractive index," U.S. patent 6,158,244 (December 12, 2000).
31. Q. Zhu and Y. Fu, Ann. Phys. **527**, 205 (2015).